Imaging Inflammation in Atherosclerosis with CXCR4-Directed ^{68}Ga-Pentixafor PET/CT: Correlation with ^{18}F-FDG PET/CT

Malte Kircher[1], Johannes Tran-Gia[1], Luisa Kemmer[1], Xiaoli Zhang[2], Andreas Schirbel[1], Rudolf A. Werner[1], Andreas K. Buck[1], Hans-Jürgen Wester[3], Marcus Hacker[4], Constantin Lapa*[1], and Xiang Li*[2,4]

[1]*Department of Nuclear Medicine, University Hospital Würzburg, Würzburg, Germany;* [2]*Department of Nuclear Medicine, Beijing Anzhen Hospital, Capital Medical University, Beijing, China;* [3]*Pharmaceutical Radiochemistry, Technische Universität München, Munich, Germany; and* [4]*Division of Nuclear Medicine, Department of Biomedical Imaging and Image-Guided Therapy, Medical University of Vienna, Vienna, Austria*

C-X-C motif chemokine receptor 4 (CXCR4) is expressed on the surface of various cell types involved in atherosclerosis, with a particularly rich receptor expression on macrophages and T cells. First pilot studies with ^{68}Ga-pentixafor, a novel CXCR4-directed PET tracer, have shown promise to noninvasively image inflammation within atherosclerotic plaques. The aim of this retrospective study was to investigate the performance of ^{68}Ga-pentixafor PET/CT for imaging atherosclerosis in comparison to ^{18}F-FDG PET/CT. **Methods:** Ninety-two patients (37 women and 55 men; mean age, 62 ± 10 y) underwent ^{68}Ga-pentixafor and ^{18}F-FDG PET/CT for staging of oncologic diseases. In these subjects, lesions in the walls of large arteries were identified using morphologic and PET criteria for atherosclerosis ($n = 652$). Tracer uptake was measured and adjusted for vascular lumen (background) signal by calculation of target-to-background ratios (TBRs) by 2 investigators masked to the other PET scan. On a lesion-to-lesion and patient basis, the TBRs of both PET tracers were compared and additionally correlated to the degree of arterial calcification as quantified in CT. **Results:** On a lesion-to-lesion basis, ^{68}Ga-pentixafor and ^{18}F-FDG uptake showed a weak correlation ($r = 0.28$; $P < 0.01$). ^{68}Ga-pentixafor PET identified more lesions ($n = 290$; TBR ≥ 1.6, $P < 0.01$) and demonstrated higher uptake than ^{18}F-FDG PET (1.8 ± 0.5 vs. 1.4 ± 0.4; $P < 0.01$). The degree of plaque calcification correlated negatively with both ^{68}Ga-pentixafor and ^{18}F-FDG uptake ($r = -0.38$ vs. -0.31, both $P < 0.00001$). **Conclusion:** CXCR4-directed imaging of the arterial wall with ^{68}Ga-pentixafor PET/CT identified more lesions than ^{18}F-FDG PET/CT, with only a weak correlation between tracers. Further studies to elucidate the underlying biologic mechanisms and sources of CXCR4 positivity, and to investigate the clinical utility of chemokine receptor–directed imaging of atherosclerosis, are highly warranted.

Key Words: atherosclerotic lesions; plaque; molecular imaging; CXCR4; FDG

J Nucl Med 2020; 61:751–756
DOI: 10.2967/jnumed.119.234484

Despite significant improvement in the management of cardiovascular diseases, coronary artery disease and stroke are still the leading causes of mortality in developed societies (*1,2*). Atherosclerosis, the common underlying pathogenesis, is characterized by the gradual formation of focal, asymmetric arterial wall lesions that progressively narrow the affected vascular lumen (*3*). Formation of an atherosclerotic lesion is initiated by endothelial dysfunction, followed by chronic accumulation of lipids, triggering a chemotaxis-orchestrated migration of atherogenic, proinflammatory immune cells to the lesion (*3–5*). Structurally unstable plaques are prone to rupture, leading to thrombosis and possibly severe complications such as myocardial infarction or stroke (*6*). Though many of the exact mechanisms of plaque formation and rupture are yet to be elucidated, inflammation is considered one of the most important predictive factors for stroke or myocardial infarction due to atherosclerotic plaque ruptures (*7*). This hypothesis was recently validated by a trial in which antiinflammatory therapy with the interleukin-1β inhibitor canakinumab significantly lowered rates of cardiovascular events (*8*).

Functional imaging of arterial inflammation can help to identify patients at risk of plaque rupture (*9*). PET has been used to visualize different aspects of the atherosclerotic plaque and its associated inflammation, with most PET tracers targeting activated macrophages within the atherosclerotic lesion (*10,11*), and with ^{18}F-FDG being the most-studied tracer of nuclear inflammation imaging (*12–14*). Other approaches include the use of ^{18}F-NaF, which can detect calcifications and microcalcifications (*15–17*). Imaging atherosclerosis with PET/CT not only characterizes atherosclerotic plaques on a molecular level but also enables the quantification of arterial calcification (*11*), combining the strengths of both modalities.

Chemokine-mediated recruitment of proinflammatory leukocytes to the dysfunctional endothelium and subsequent plaque formation are important steps in atheroprogression (*3*). C-X-C motif chemokine receptor 4 (CXCR4) and its endogenous ligands, C-X-C motif chemokine 12 (CXCL12; stromal cell–derived factor 1) and migration inhibitory factor, play important roles in progenitor and immune cell trafficking (*18*). The precise role of the CXCR4/CXCL12 axis in atherosclerosis progression is yet to be fully elucidated, with conflicting reports about atherogenic and atheroprotective effects, respectively (*18*). This conflict is partly due to the recent identification of migration inhibitory factor as an alternate ligand for

Received Jul. 25, 2019; revision accepted Sep. 27, 2019.
For correspondence or reprints contact: Constantin Lapa, Department of Nuclear Medicine, University Hospital Würzburg, Oberdürrbacher Strasse 6, 97080 Würzburg, Germany.
E-mail: lapa_c@ukw.de
*Contributed equally to this work.
Published online Oct. 25, 2019.

CXCR4 (*19*). Evidence shows that CXCR4 activation by CXCL12 exerts stabilizing effects on atherosclerotic lesions, whereas migration inhibitory factor acts as a major proinflammatory player (*20*).

Recently, CXCR4-directed PET imaging with ^{68}Ga-pentixafor introduced the possibility for noninvasive, in vivo visualization of human CXCR4 expression (*21–25*). First pilot studies examining its ability to characterize atherosclerotic inflammation and myocardial injury have shown promising results and have suggested that major parts of the PET signal originate from intralesional macrophages (*26–31*). In this study, we investigated the performance of ^{68}Ga-pentixafor for detection of arterial wall inflammation in comparison to ^{18}F-FDG and correlated the respective tracer uptake to the degree of calcification in the corresponding lesions.

MATERIALS AND METHODS

Patients

One hundred forty-four oncologic patients underwent PET/CT imaging with ^{68}Ga-pentixafor and ^{18}F-FDG (with a maximum interval of 3 d between the 2 scans) for staging purposes or for evaluation of CXCR4-directed endoradiotherapy (*32,33*). Subjects with a history of inflammatory diseases (including vasculitis), chemotherapy in the preceding 4 wk, or cardiovascular events (myocardial infarction, stroke) in the last 6 mo, and patients taking cholesterol-lowering drugs such as statins or ezetimibe, were excluded from the study ($n = 52$). The remaining 92 subjects (37 women and 55 men; mean age, 62 ± 10 y; 33 with multiple myeloma, 25 with adrenocortical carcinoma, 13 with neuroendocrine neoplasia, 6 with non–small cell lung cancer, and 15 with miscellaneous other conditions) were included in this retrospective analysis. A flowchart of the study design is shown in Supplemental Figure 1 (supplemental materials are available at http://jnm.snmjournals.org).

^{68}Ga-pentixafor was administered in compliance with the German Medicinal Products Act, AMG §13 2b, and in accordance with the responsible regulatory body (Government of Upper Franconia, "*Regierung von Oberfranken*"). The data analysis was disclosed to the local ethics committee of Würzburg University Hospital, and the need for a formal review was waived. All patients gave written informed consent before imaging. The patient characteristics are shown in Table 1.

TABLE 1
Patient Characteristics

Characteristic	Data
Patients (*n*)	92
Sex (*n*)	
Male	55
Female	37
Age (y)	62 ± 10
Body mass index (kg/m^2)	26.0
Cardiovascular risk factors (*n*)	
History of cardiovascular disease	32 (35%)
Hypertension	56 (61%)
Diabetes	9 (10%)
Nicotine abuse	27 (29%)
Obesity	16 (17%)
C-reactive protein (≥3 mg/L)	18 (20%)
Medication at time of imaging (*n*)	
Angiotensin-converting enzyme inhibitor	25 (27%)
β-blocker	26 (28%)
Calcium channel antagonist	25 (27%)
Diuretic	19 (21%)
Angiotensin I receptor antagonists	9 (10%)
Coagulation inhibitors	34 (37%)
Type of disease (*n*)	
Multiple myeloma	33 (36%)
Adrenocortical cancer	25 (27%)
Neuroendocrine tumor	13 (14%)
Non-small cell lung cancer	6 (7%)
Pleural mesothelioma	4 (4%)
Lymphoma	3 (3%)
Stomach cancer	2 (2%)
Hepatocellular carcinoma	1 (1%)
T-cell non-Hodgkin lymphoma	1 (1%)
Small cell lung cancer	1 (1%)
Pancreatic cancer	1 (1%)
Thyroid cancer	1 (1%)
Diffuse large B-cell lymphoma	1 (1%)

PET/CT Acquisition

All ^{68}Ga-pentixafor and ^{18}F-FDG PET/CT scans were performed on a dedicated PET/CT scanner (Biograph mCT 64; Siemens Medical Solutions). ^{18}F-FDG PET/CT imaging was performed after a 6-h fasting period to ensure serum glucose levels below 130 mg/dL. Injected activities ranged from 108 to 178 MBq (mean, 143 ± 26 MBq) for ^{68}Ga-pentixafor and from 235 to 363 MBq (mean, 299 ± 18 MBq) for ^{18}F-FDG.

Low-dose CT scans for attenuation correction were acquired (35 mAs, 120 keV, a 512 × 512 matrix, 5-mm slice thickness, increment of 30 mm/s, rotation time of 0.5 s, and pitch index of 0.8). Whole-body (top of the skull to knees) scans were performed 1 h after administration of the radiopharmaceutical. All PET images were reconstructed using standard parameters (HD-PET [Siemens]; 3 iterations, 24 subsets, 2-mm gaussian filtering, 5-mm axial resolution, 4 × 4 mm^2 in-plane resolution) with corrections for attenuation (CT-based), dead time, random events, and scatter. The PET scanner is periodically checked for calibration accuracy as part of quality control according to published guidelines (*34*).

Data Analysis

Images were analyzed by 2 investigators masked to the other PET scan. ^{68}Ga-pentixafor and ^{18}F-FDG uptake was visually and semiquantitatively assessed with commercially available software (Hybrid 3D; Hermes Medical Solutions) on transaxial PET, CT, and PET/CT slices. The following segments of large arteries were analyzed for signs of atherosclerosis in each patient: the left and right carotid arteries; the ascending thoracic aorta; the aortic arch; the descending thoracic aorta; the abdominal aorta; and the left and right iliac arteries. Signs of atherosclerosis were defined as either arterial wall calcification with a minimum density of 130 Hounsfield units (HU) on unenhanced CT images or high focal tracer uptake on either ^{18}F-FDG or ^{68}Ga-pentixafor PET images, defined as a minimum arterial target-to-background ratio (TBR) of 1.6, as described for ^{18}F-FDG PET in the literature (*35*).

Volumes of interest were manually drawn at the selected sites, particularly at regions of arterial bifurcations, known to be susceptible to atherosclerotic formation, and at calcified arterial wall lesions. For

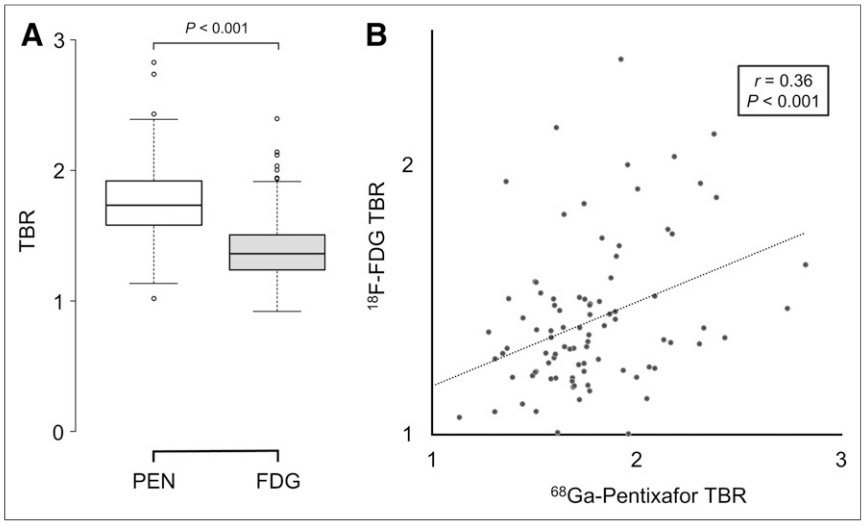

FIGURE 1. Comparison of ^{68}Ga-pentixafor and ^{18}F-FDG uptake on per-patient basis. Box plot (A) and scatterplot (B) showing correlation of mean ^{18}F-FDG and ^{68}Ga-pentixafor (PEN) uptake as measured by TBR on per-patient basis.

analysis of calcification extent, lesions were categorized according to the modified Agatston score (*36*), with measurements of HU on unenhanced CT images. Group 1 (noncalcified lesions) had a calcium density of less than 130 HU. Group 2 (mildly calcified lesions) had a calcium density of 130–399 HU. Group 3 (severely calcified lesions) had a calcium density of at least 400 HU.

TBRs were calculated as previously described (*35*). First, SUV_{max} was measured by placing a circular 10-mm volume of interest around a site of focal uptake. Then, the SUV_{mean} of the background was derived by calculating the mean of 3 regions of interest placed in the superior vena cava (the SUV of the blood pool). TBRs were then calculated as SUV_{max} (focal uptake) divided by the SUV of the blood pool.

Statistics

All statistical testing was performed in SPSS statistics 25 (IBM Corp.). Kolmogorov–Smirnov testing was used to verify a normal distribution of the data. Continuous parametric variables are expressed as mean ± SD. For group statistics, comparisons within the 3 groups of lesions were performed using 1-way ANOVA. The significance of observed differences between groups was confirmed with a Games–Howell post hoc test. Unpaired *t* tests were used to compare uptake (ratios) of both tracers in corresponding lesions. Pearson correlation coefficients (*r*) were calculated to assess the association between the TBRs of both tracers. *P* values of at least 0.05 were considered statistically significant.

RESULTS

Comparison of ^{68}Ga-Pentixafor and ^{18}F-FDG Uptake: Patient-Based Analysis

In the patient-based analysis, 88 of 92 subjects (95.7%) had at least 1 ^{68}Ga-pentixafor–positive lesion and 58 patients (63.0%) had at least 1 ^{18}F-FDG–positive lesion. Two patients (2.2%) had both negative ^{68}Ga-pentixafor and negative ^{18}F-FDG scans, and 2 patients (2.2%) had exclusively ^{18}F-FDG–positive lesions. In the remaining 32 subjects (34.8%), all lesions were ^{68}Ga-pentixafor–positive, ^{18}F-FDG–negative.

The median number of ^{68}Ga-pentixafor–positive lesions (per patient) was 4 (range, 0–13), as compared with 1 for ^{18}F-FDG (range, 0–10). The number of ^{68}Ga-pentixafor–positive lesions moderately correlated with the number of ^{18}F-FDG–positive lesions ($r = 0.46$, $P < 0.0001$). On a patient level, individual mean TBRs for ^{68}Ga-pentixafor were significantly higher than those for ^{18}F-FDG (1.8 ± 0.3 vs. 1.4 ± 0.3; $P < 0.001$; Fig. 1) and were only moderately correlated ($r = 0.36$, $P < 0.001$; Fig. 1).

Comparison of ^{68}Ga-Pentixafor and ^{18}F-FDG Uptake: Lesion-Based Analysis

In total, 652 sites of arterial wall calcification or elevated tracer uptake (TBR ≥ 1.6) were identified and selected for further analysis. At these sites, mean SUV_{max} was significantly higher for ^{68}Ga-pentixafor than for ^{18}F-FDG (3.3 ± 1.0 vs. 2.6 ± 0.7; $P < 0.01$). Both tracers' SUV_{max} showed a moderate positive correlation ($r = 0.43$; $P < 0.01$). With the mean blood-pool SUV of ^{68}Ga-pentixafor and ^{18}F-FDG being comparable (1.87 ± 0.37 vs. 1.81 ± 0.29, $P = 0.18$), the mean TBR was significantly higher for ^{68}Ga-pentixafor than for ^{18}F-FDG (1.8 ± 0.5 vs. 1.4 ± 0.4; $P < 0.01$). The TBR of ^{68}Ga-pentixafor and ^{18}F-FDG showed a weak positive correlation ($r = 0.28$, $P < 0.01$; Fig. 2). When a TBR threshold of 1.6 was applied, 290 of the potential lesions were exclusively identified on ^{68}Ga-pentixafor PET (^{18}F-FDG < 1.6 and ^{68}Ga-pentixafor ≥ 1.6, $P < 0.01$). An example of the different tracer uptake patterns is given in Figure 3.

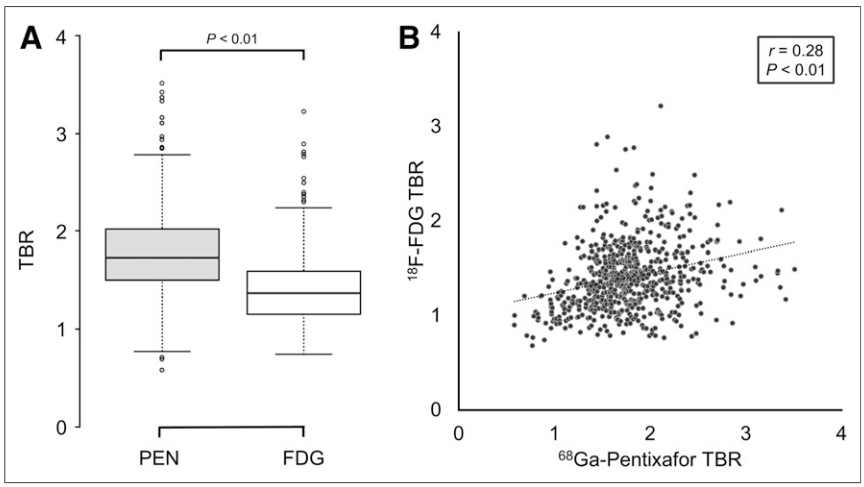

FIGURE 2. Comparison of ^{68}Ga-pentixafor and ^{18}F-FDG uptake on lesion-to-lesion basis. Box plot (A) and scatterplot (B) showing correlation of ^{18}F-FDG and ^{68}Ga-pentixafor (PEN) uptake as measured by TBR.

Relationship Between Plaque Calcification and Tracer Uptake

Most of the 652 analyzed sites demonstrated no signs of calcification (<130 HU; $n = 467$),

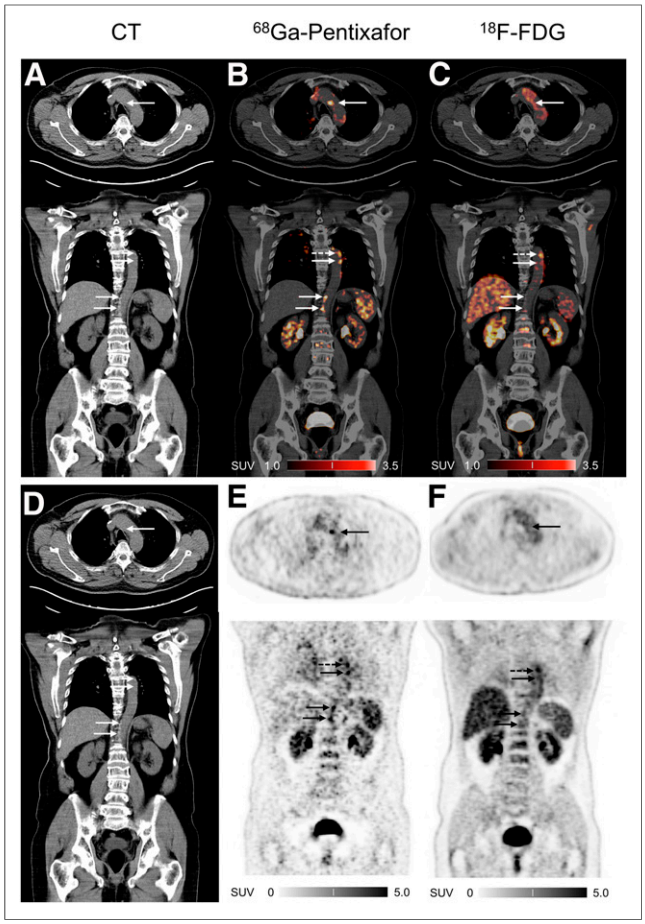

FIGURE 3. Example of concordant and discordant ^{68}Ga-pentixafor and ^{18}F-FDG uptake. Representative transversal and coronal CT (A and D), ^{68}Ga-pentixafor PET/CT (B), and ^{18}F-FDG PET/CT (C), as well as respective PET-only (E and F), images of patient with multiple myeloma. Dashed arrows indicate concordant foci of ^{68}Ga-pentixafor and ^{18}F-FDG arterial uptake; solid arrows show lesions exclusively seen in ^{68}Ga-pentixafor but not in ^{18}F-FDG PET.

whereas 99 lesions showed mild calcification (130–399 HU) and 86 showed severe calcification (≥400 HU).

There was an inverse relationship between the extent of calcification and the intensity of tracer uptake as measured by TBR for both ^{68}Ga-pentixafor and ^{18}F-FDG. Severely calcified lesions ($n = 86$) showed the lowest TBRs for both PET tracers (1.4 ± 0.6 and 1.1 ± 0.4 for ^{68}Ga-pentixafor and ^{18}F-FDG, respectively). Mildly calcified lesions ($n = 99$) showed higher TBRs than severely calcified lesions (1.7 ± 0.4 and 1.3 ± 0.3, respectively; $P < 0.01$). The highest TBRs were concordantly observed in noncalcified lesions ($n = 467$; 1.9 ± 0.4 and 1.5 ± 0.4, respectively). Higher TBRs for ^{68}Ga-pentixafor than for ^{18}F-FDG were also observed when the different calcification subgroups were analyzed. Results are shown in Figure 4.

DISCUSSION

^{18}F-FDG is the best-studied PET tracer for inflammation imaging and is routinely used for nuclear imaging of atherosclerosis (*10*). More recently, several small-animal and human pilot studies have established the feasibility of the CXCR4-directed PET tracer ^{68}Ga-pentixafor for cardiovascular imaging (*26–30,37*).

^{68}Ga-Pentixafor and ^{18}F-FDG Uptake Show Only a Weak Correlation

Overall, accumulation of ^{68}Ga-pentixafor and ^{18}F-FDG showed only a weak correlation. This was primarily observed in noncalcified lesions, in which many sites with focal ^{68}Ga-pentixafor uptake were inconspicuous on ^{18}F-FDG PET. Most of the ^{18}F-FDG signal can be attributed to activated, proinflammatory macrophages (*10*). Likewise, at least part of the ^{68}Ga-pentixafor signal is traceable to areas rich in CD68-positive macrophages (*28,38*), which may account for the lesions identified by both tracers. However, the dynamics of CXCR4 regulation in atherosclerosis are complex, and various involved cell types (including thrombocytes) have been described as contributing to the ^{68}Ga-pentixafor signal (*18,31,39,40*), making its interpretation more challenging than ^{18}F-FDG.

The ^{68}Ga-Pentixafor Signal Appears to Originate Not Merely from Inflammation

Although there has been extensive research into the CXCR4-CXCL12 axis and its role in atherosclerosis, the basis of its involvement is still incompletely understood, given the contribution of multiple cell types and a rather complex and highly dynamic receptor expression profile (*20*). Because ^{68}Ga-pentixafor PET/CT detects sites that are inconspicuous on ^{18}F-FDG PET/CT, the source of the PET signal probably originates in additional cell types beyond mere inflammation (*41*). In the setting of atherosclerosis, CXCR4-expressing cells include T cells, thrombocytes, and smooth muscle cells; thus, some of the exclusively ^{68}Ga-pentixafor–positive sites might represent very early stage lesions without markedly elevated inflammation.

It is the prevailing scientific consensus that the effects of CXCR4 through activation by its cognate ligand CXCL12 are largely atheroprotective, particularly by maintaining the arterial wall integrity, which prevents vascular remodeling. Maintenance of wall integrity is achieved by protecting the endothelial barrier function and smooth muscle cell elasticity, which is associated with retarding adhesion and penetration of leukocytes into the arterial intima (*39*). Collagen produced by smooth muscle cells strengthens the fibrous plaque cap, implying that dysfunctional smooth muscle cells lead to reduced plaque stability, which in turn increases the risk of subsequent plaque rupture and thrombosis (*42*). On the other hand, observations suggest that CXCR4 activation through its noncognate-ligand migration inhibitory factor leads to recruitment of highly inflammatory immune cells, including monocytes, macrophages, and T cells, and has a detrimental effect on atheroprogression and plaque stability (*19*).

One study of carotid plaques in humans showed that compared with unaffected vessels, CXCR4 expression is likewise elevated in both stable and unstable atherosclerotic plaques, with the highest receptor expression found on macrophages and macrophage-derived foam cells (*31*). This observation was also made in another study that showed an abundant accumulation of ^{68}Ga-pentixafor, especially in inflamed plaques, verified histologically in human carotid plaques and in a rabbit model (*28*). Taken together, preclinical and clinical findings suggest a sophisticated system of CXCR4-expressing cell types within the atherosclerotic lesion that, depending on their activating ligand, may have atherogenic or antiatherosclerotic effects.

Tracer Uptake and Plaque Calcification

Our data show an inverse relationship between both ^{68}Ga-pentixafor and ^{18}F-FDG uptake and the degree of calcification. Noncalcified sites demonstrated the highest, severely calcified plaques the

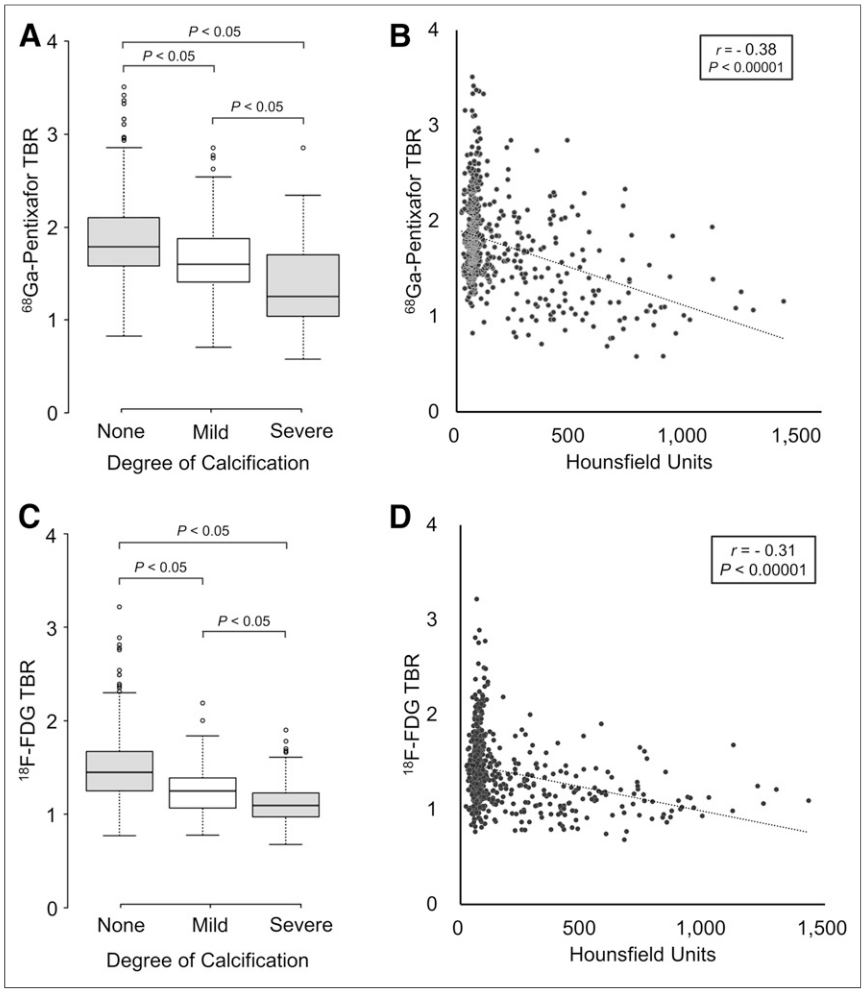

FIGURE 4. ^{68}Ga-pentixafor and ^{18}F-FDG uptake in correlation to degree of calcification on lesion-to-lesion basis. Correlation of ^{68}Ga-pentixafor (A and B) and ^{18}F-FDG (C and D) uptake with degree of calcification. Lesions were categorized by calcification degree as noncalcified (<130 HU), mildly calcified (130–399 HU), or severely calcified (≥400 HU), respectively. TBR of ^{68}Ga-pentixafor and ^{18}F-FDG are lowest in severely calcified lesions and highest in noncalcified lesions.

lowest TBRs for both tracers, respectively. Severely calcified plaques are generally considered to be more stable and less susceptible to rupture. In the case of ^{18}F-FDG, this observation is consistent with previously published studies (*13,43*). Regarding ^{68}Ga-pentixafor, Weiberg et al. recently documented similar results using ^{68}Ga-pentixafor PET/CT for atherosclerosis imaging, with increased tracer uptake in only a few of the calcified lesions (*30*).

Limitations

There are several limitations to this retrospective study. The first concerns the cohort of oncologic, non–cardiovascular-disease patients and the PET acquisition protocol used. The impact of previous anticancer therapies on vascular inflammation cannot be excluded (although chemotherapy within 4 wk before imaging was an exclusion criterion). In addition, metabolic (inflammatory) changes induced by malignancy itself cannot be measured and therefore confound the results of this pilot study. Given the fact that imaging was performed on oncology patients, scans were started as early as 1 h after tracer injection, limiting the diagnostic accuracy, as tracer circulation time is a critical variable affecting quantification of plaque uptake (*35*). This limitation is particularly true for ^{68}Ga-pentixafor, for which experience with inflammation imaging is limited. Comparability between tracers might furthermore be influenced by differences in biodistribution. Studies to optimize the imaging protocol are needed. The use of an unestablished, nonvalidated TBR threshold to define ^{68}Ga-pentixafor–positive lesions is another limitation. In the limited literature available, the mean TBR of atherosclerotic lesions in the carotid arteries were 1.6 (*38*), 1.7 (*30*), and 1.6 (*28,* supplemental data), suggesting that the chosen threshold might be a reasonable first estimate, but further studies are needed to define the correct threshold for the detection of CXCR4-positive plaques visualized by receptor-directed PET imaging.

The second major limitation concerns the lack of a gold standard, namely the lack of histopathologic confirmation of an atherosclerotic plaque and associated cell types. Although the colocalization of CD68 (macrophages) and CXCR4 within atherosclerotic plaques observed in prior studies suggests that at least part of the PET signal originates from macrophages (*28,31,38*), no definitive conclusions can be drawn about its exact cellular source, as it is the sum of all CXCR4-expressing cells localized within or near a particular lesion and may include a combination of various cell types, including T-cells, thrombocytes, and smooth muscle cells (*18,31,39,41*).

The third major limitation concerns the radiopharmaceutical itself. The use of ^{68}Ga-labeled tracers for vascular PET imaging poses several physical and technical challenges, as the high positron energy and high positron range of ^{68}Ga lead to noisier images and worse spatial resolution, which are amplified by the lower injected activity of ^{68}Ga compared with ^{18}F-FDG. Therefore, it cannot be ruled out that the increased number of foci observed with ^{68}Ga-pentixafor PET is (at least partially) attributable to noise (*44*). These limitations are partly compensated by the predominantly high specificity of most ^{68}Ga-labeled radiopharmaceuticals in comparison to the nonspecific tissue uptake of ^{18}F-labeled FDG (*45*). In addition, ^{68}Ga-labeled tracers have already been successfully used to image atherosclerotic plaques in vessels as small as the coronary arteries (*46*), and the general feasibility of plaque imaging with ^{68}Ga-pentixafor PET in particular has been demonstrated in recent studies (*30,38*). The reproducibility of the data was not tested in this retrospective study.

CONCLUSION

CXCR4-directed imaging of the arterial wall with ^{68}Ga-pentixafor PET/CT identified more lesions than ^{18}F-FDG PET/CT, with only a weak correlation between tracers. Further studies to elucidate the underlying biologic mechanisms and sources of CXCR4 positivity and to investigate the clinical utility of chemokine receptor–directed imaging of atherosclerosis are highly warranted.

DISCLOSURE

Hans-Jürgen Wester is founder and shareholder of Scintomics. No other potential conflict of interest relevant to this article was reported.

KEY POINTS

QUESTION: Is CXCR4-directed ^{68}Ga-pentixafor PET/CT able to image inflammation in atherosclerosis, and how does it compare with ^{18}F-FDG PET/CT?

PERTINENT FINDINGS: In a cohort of 92 oncologic patients, ^{68}Ga-pentixafor PET/CT identified more lesions with higher target-to-background contrast than ^{18}F-FDG PET/CT.

IMPLICATIONS FOR PATIENT CARE: Imaging of CXCR4 expression might contribute to a better understanding of the dynamics of atheroprogression and plaque destabilization and, in the future, might help identify patients at risk of cardiovascular events.

REFERENCES

1. Pant S, Deshmukh A, Gurumurthy GS, et al. Inflammation and atherosclerosis: revisited. *J Cardiovasc Pharmacol Ther.* 2014;19:170–178.
2. Benjamin EJ, Virani SS, Callaway CW, et al. Heart disease and stroke statistics: 2018 update—a report from the American Heart Association. *Circulation.* 2018;137: e67–e492.
3. Weber C, Noels H. Atherosclerosis: current pathogenesis and therapeutic options. *Nat Med.* 2011;17:1410–1422.
4. Hansson GK, Hermansson A. The immune system in atherosclerosis. *Nat Immunol.* 2011;12:204–212.
5. Moore KJ, Tabas I. Macrophages in the pathogenesis of atherosclerosis. *Cell.* 2011;145:341–355.
6. Finn AV, Nakano M, Narula J, Kolodgie FD, Virmani R. Concept of vulnerable/unstable plaque. *Arterioscler Thromb Vasc Biol.* 2010;30:1282–1292.
7. Libby P, Ridker PM, Hansson GK. Progress and challenges in translating the biology of atherosclerosis. *Nature.* 2011;473:317–325.
8. Ridker PM, Everett BM, Thuren T, et al. Antiinflammatory therapy with canakinumab for atherosclerotic disease. *N Engl J Med.* 2017;377:1119–1131.
9. Rudd JH, Hyafil F, Fayad ZA. Inflammation imaging in atherosclerosis. *Arterioscler Thromb Vasc Biol.* 2009;29:1009–1016.
10. Joseph P, Tawakol A. Imaging atherosclerosis with positron emission tomography. *Eur Heart J.* 2016;37:2974–2980.
11. Tarkin JM, Dweck MR, Evans NR, et al. Imaging atherosclerosis. *Circ Res.* 2016;118: 750–769.
12. Tawakol A, Migrino RQ, Bashian GG, et al. In vivo ^{18}F-fluorodeoxyglucose positron emission tomography imaging provides a noninvasive measure of carotid plaque inflammation in patients. *J Am Coll Cardiol.* 2006;48:1818–1824.
13. Li X, Heber D, Cal-Gonzalez J, et al. Association between osteogenesis and inflammation during the progression of calcified plaque evaluated by ^{18}F-fluoride and ^{18}F-FDG. *J Nucl Med.* 2017;58:968–974.
14. Li X, Heber D, Rausch I, et al. Quantitative assessment of atherosclerotic plaques on ^{18}F-FDG PET/MRI: comparison with a PET/CT hybrid system. *Eur J Nucl Med Mol Imaging.* 2016;43:1503–1512.
15. Moghbel M, Al-Zaghal A, Werner TJ, Constantinescu CM, Hoilund-Carlsen PF, Alavi A. The role of PET in evaluating atherosclerosis: a critical review. *Semin Nucl Med.* 2018;48:488–497.
16. Oliveira-Santos M, Castelo-Branco M, Silva R, et al. Atherosclerotic plaque metabolism in high cardiovascular risk subjects: a subclinical atherosclerosis imaging study with ^{18}F-NaF PET-CT. *Atherosclerosis.* 2017;260:41–46.
17. Irkle A, Vesey AT, Lewis DY, et al. Identifying active vascular microcalcification by ^{18}F-sodium fluoride positron emission tomography. *Nat Commun.* 2015;6:7495.
18. Döring Y, Pawig L, Weber C, Noels H. The CXCL12/CXCR4 chemokine ligand/receptor axis in cardiovascular disease. *Front Physiol.* 2014;5:212.
19. Bernhagen J, Krohn R, Lue H, et al. MIF is a noncognate ligand of CXC chemokine receptors in inflammatory and atherogenic cell recruitment. *Nat Med.* 2007;13:587–596.
20. Schmitt MM, Megens RT, Zernecke A, et al. Endothelial junctional adhesion molecule-A guides monocytes into flow-dependent predilection sites of atherosclerosis. *Circulation.* 2014;129:66–76.
21. Lapa C, Schreder M, Schirbel A, et al. [^{68}Ga]pentixafor-PET/CT for imaging of chemokine receptor CXCR4 expression in multiple myeloma: comparison to [^{18}F]FDG and laboratory values. *Theranostics.* 2017;7:205–212.
22. Lapa C, Luckerath K, Rudelius M, et al. [^{68}Ga]pentixafor-PET/CT for imaging of chemokine receptor 4 expression in small cell lung cancer: initial experience. *Oncotarget.* 2016;7:9288–9295.
23. Vag T, Gerngross C, Herhaus P, et al. First experience with chemokine receptor CXCR4-targeted PET imaging of patients with solid cancers. *J Nucl Med.* 2016;57:741–746.
24. Wester HJ, Keller U, Schottelius M, et al. Disclosing the CXCR4 expression in lymphoproliferative diseases by targeted molecular imaging. *Theranostics.* 2015;5:618–630.
25. Philipp-Abbrederis K, Herrmann K, Knop S, et al. In vivo molecular imaging of chemokine receptor CXCR4 expression in patients with advanced multiple myeloma. *EMBO Mol Med.* 2015;7:477–487.
26. Lapa C, Reiter T, Werner RA, et al. [^{68}Ga]pentixafor-PET/CT for imaging of chemokine receptor 4 expression after myocardial infarction. *JACC Cardiovasc Imaging.* 2015;8:1466–1468.
27. Thackeray JT, Derlin T, Haghikia A, et al. Molecular imaging of the chemokine receptor CXCR4 after acute myocardial infarction. *JACC Cardiovasc Imaging.* 2015;8:1417–1426.
28. Hyafil F, Pelisek J, Laitinen I, et al. Imaging the cytokine receptor CXCR4 in atherosclerotic plaques with the radiotracer ^{68}Ga-pentixafor for PET. *J Nucl Med.* 2017;58:499–506.
29. Reiter T, Kircher M, Schirbel A, et al. Imaging of C-X-C motif chemokine receptor CXCR4 expression after myocardial infarction with [^{68}Ga]pentixafor-PET/CT in correlation with cardiac MRI. *JACC Cardiovasc Imaging.* 2018;11:1541–1543.
30. Weiberg D, Thackeray JT, Daum G, et al. Clinical molecular imaging of chemokine receptor CXCR4 expression in atherosclerotic plaque using ^{68}Ga-pentixafor PET: correlation with cardiovascular risk factors and calcified plaque burden. *J Nucl Med.* 2018;59:266–272.
31. Merckelbach S, van der Vorst EPC, Kallmayer M, et al. Expression and cellular localization of CXCR4 and CXCL12 in human carotid atherosclerotic plaques. *Thromb Haemost.* 2018;118:195–206.
32. Lapa C, Herrmann K, Schirbel A, et al. CXCR4-directed endoradiotherapy induces high response rates in extramedullary relapsed multiple myeloma. *Theranostics.* 2017;7:1589–1597.
33. Lapa C, Hanscheid H, Kircher M, et al. Feasibility of CXCR4-directed radioligand therapy in advanced diffuse large B-cell lymphoma. *J Nucl Med.* 2019;60:60–64.
34. Aide N, Lasnon C, Veit-Haibach P, Sera T, Sattler B, Boellaard R. EANM/EARL harmonization strategies in PET quantification: from daily practice to multicentre oncological studies. *Eur J Nucl Med Mol Imaging.* 2017;44:17–31.
35. Bucerius J, Hyafil F, Verberne HJ, et al. Position paper of the Cardiovascular Committee of the European Association of Nuclear Medicine (EANM) on PET imaging of atherosclerosis. *Eur J Nucl Med Mol Imaging.* 2016;43:780–792.
36. Agatston AS, Janowitz WR, Hildner FJ, Zusmer NR, Viamonte M Jr, Detrano R. Quantification of coronary artery calcium using ultrafast computed tomography. *J Am Coll Cardiol.* 1990;15:827–832.
37. Greenland P, LaBree L, Azen SP, Doherty TM, Detrano RC. Coronary artery calcium score combined with Framingham score for risk prediction in asymptomatic individuals. *JAMA.* 2004;291:210–215.
38. Li X, Yu W, Wollenweber T, et al. [^{68}Ga]pentixafor PET/MR imaging of chemokine receptor 4 expression in the human carotid artery. *Eur J Nucl Med Mol Imaging.* 2019;46:1616–1625.
39. Döring Y, Noels H, van der Vorst EPC, et al. Vascular CXCR4 limits atherosclerosis by maintaining arterial integrity: evidence from mouse and human studies. *Circulation.* 2017;136:388–403.
40. Grosse GM, Bascunana P, Schulz-Schaeffer WJ, et al. Targeting chemokine receptor CXCR4 and translocator protein for characterization of high-risk plaque in carotid stenosis ex vivo. *Stroke.* 2018;49:1988–1991.
41. Zernecke A, Weber C. Chemokines in atherosclerosis: proceedings resumed. *Arterioscler Thromb Vasc Biol.* 2014;34:742–750.
42. O'Connor SD, Graffy PM, Zea R, Pickhardt PJ. Does nonenhanced CT-based quantification of abdominal aortic calcification outperform the Framingham risk score in predicting cardiovascular events in asymptomatic adults? *Radiology.* 2019;290:108–115.
43. Derlin T, Toth Z, Papp L, et al. Correlation of inflammation assessed by ^{18}F-FDG PET, active mineral deposition assessed by ^{18}F-fluoride PET, and vascular calcification in atherosclerotic plaque: a dual-tracer PET/CT study. *J Nucl Med.* 2011;52:1020–1027.
44. Derlin T, Thiele J, Weiberg D, et al. Evaluation of ^{68}Ga-glutamate carboxypeptidase II ligand positron emission tomography for clinical molecular imaging of atherosclerotic plaque neovascularization. *Arterioscler Thromb Vasc Biol.* 2016;36: 2213–2219.
45. Sanchez-Crespo A. Comparison of gallium-68 and fluorine-18 imaging characteristics in positron emission tomography. *Appl Radiat Isot.* 2013;76:55–62.
46. Derlin T, Sedding DG, Dutzmann J, et al. Imaging of chemokine receptor CXCR4 expression in culprit and nonculprit coronary atherosclerotic plaque using motion-corrected [^{68}Ga]pentixafor PET/CT. *Eur J Nucl Med Mol Imaging.* 2018;45:1934–1944.